



ELSEVIER

Contents lists available at ScienceDirect

# Nuclear Instruments and Methods in Physics Research A

journal homepage: [www.elsevier.com/locate/nima](http://www.elsevier.com/locate/nima)

## The SAFIR experiment: Concept, status and perspectives



Robert Becker<sup>a</sup>, Alfred Buck<sup>b</sup>, Chiara Casella<sup>a,\*</sup>, Günther Dissertori<sup>a</sup>, Jannis Fischer<sup>a</sup>, Alexander Howard<sup>a</sup>, Mikiko Ito<sup>a</sup>, Parisa Khateri<sup>a</sup>, Werner Lustermann<sup>a</sup>, Josep F. Oliver<sup>c</sup>, Ulf Röser<sup>a</sup>, Geoffrey Warnock<sup>d</sup>, Bruno Weber<sup>d</sup>

<sup>a</sup> Institute for Particle Physics, ETH Zürich, Switzerland

<sup>b</sup> Division of Nuclear Medicine, Zürich University Hospital, Switzerland

<sup>c</sup> Instituto de Fisica Corpuscular, UV-CSIC, Valencia, Spain

<sup>d</sup> Institute of Pharmacology and Toxicology, University of Zürich, Switzerland

### ARTICLE INFO

#### Article history:

Received 24 March 2016

Received in revised form

9 May 2016

Accepted 9 May 2016

Available online 13 May 2016

#### Keywords:

Positron Emission Tomography (PET)

Hybrid PET/MRI

SiPM

### ABSTRACT

The SAFIR development represents a novel Positron Emission Tomography (PET) detector, conceived for preclinical fast acquisitions inside the bore of a Magnetic Resonance Imaging (MRI) scanner. The goal is hybrid and simultaneous PET/MRI dynamic studies at unprecedented temporal resolutions of a few seconds. The detector relies on matrices of scintillating LSO-based crystals coupled one-to-one with SiPM arrays and readout by fast ASICs with excellent timing resolution and high rate capabilities. The paper describes the detector concept and the initial results in terms of simulations and characterisation measurements.

© 2016 Elsevier B.V. All rights reserved.

### 1. Introduction – hybrid PET/MRI

The development of Positron Emission Tomography (PET) detectors able to operate simultaneously with a Magnetic Resonance Imaging (MRI) scanner is a lively branch in nuclear medicine instrumentation. Despite its significant technical challenges, hybrid PET/MRI is indeed receiving a growing interest as the potentially dominating technique in the future of hybrid imaging [1].

The importance of the morphological information added to the functional PET has been undoubtedly proven by the success of PET/CT, where Computed Tomography (CT) serves as the anatomical counterpart for PET, providing – at the same time – also maps for attenuation correction [2]. With respect to the more established PET/CT technique, PET/MRI offers significant advantages, namely a better soft tissue contrast without any ionizing radiation (i.e. no additional dose delivered to the patient). The definition of the attenuation correction and the consequent quantification of PET images, on the other hand, are more challenged in PET/MRI than in PET/CT. Several different approaches are investigated to mitigate this problem [3].

PET and MRI could be used either sequentially or fully simultaneously, with time and space correlation. This latter feature represents a powerful imaging tool for e.g. moving organs and is of utmost importance for all the studies where the dynamics of the

processes is relevant, like e.g. blood flow and perfusion measurement. Recently, functional MRI (fMRI) has also gained importance, and one of the added values of simultaneous PET/MRI with respect to PET/CT is precisely the complementarity of the functional information provided by both modalities.

From an instrumentation point of view, simultaneous PET/MRI is achieved, in the vast majority of the existing approaches, with a PET detector inserted into the bore of a MR scanner. This poses challenges on the PET detector itself, both in terms of spatial constraints and in terms of mutual non-interference with the MR magnetic fields [4]. Significant progress has been done in this direction in recent years, and commercial simultaneous PET/MRI devices have started to appear in the clinical<sup>1</sup> and are soon expected also in the preclinical field.

A key point to the development of simultaneous PET/MRI systems was the development of solid state photosensors, first APDs and then SiPM, which – with their insensitivity to magnetic field, high level of compactness and (in the case of SiPM) high gain and very good timing performance – are entirely dominating the field of PET and PET/MRI instrumentation [5,6].

\* Corresponding author.

E-mail address: [chiara.casella@cern.ch](mailto:chiara.casella@cern.ch) (C. Casella).

<sup>1</sup> Examples are the Siemens Biograph mMR and the GE whole body SIGNA PET/MR.

## 2. The SAFIR experiment

### 2.1. Goal of the experiment

The goal of SAFIR – Small Animal Fast Insert for mRi – is the design, construction and characterisation of an innovative PET detector for fast and simultaneous hybrid PET/MRI imaging on small animals. The PET detector is designed specifically to be used inside the bore of the commercial 7 T Bruker BioSpec 70/30 pre-clinical MRI scanner. Differently from any other development, SAFIR aims to perform scans with ultra short acquisition durations of the order of a few seconds. This is needed in order to enable quantitative dynamic studies of fast biological processes e.g. blood perfusion and cerebral blood flow (CBF). CBF is used in fMRI as a surrogate for the neural activity, but its detailed mechanisms are still poorly understood. The golden standard tracer for CBF studies is  $^{15}\text{O}\text{-H}_2\text{O}$  (half-life of  $\sim 2$  min), and changes in activity concentrations up to 20% are expected on time scales of a few seconds, hence the need for an ultra-fast detector with high granularity temporal acquisitions.

### 2.2. Detector challenges and requirements

Beside the clear MR compatibility, SAFIR has to meet severe challenges, mostly driven by the requirement of the very high temporal resolution. In standard conditions, a short scan duration implies a poor quality in the reconstructed images, because of the lack of statistics. To compensate for the statistic losses, SAFIR must have an optimised sensitivity (i.e. a large field of view coverage) and use up to 500 MBq injected activities in the animals, which represents a one order of magnitude increase with respect to state-of-the-art preclinical systems. As a consequence, the detector readout must have high rate capabilities, in terms of rate per channel, overall bandwidth and fast DAQ system. On the other hand, a high injected activity implies also a strong random coincidences contribution, which is minimized by requiring excellent coincidence resolving time (CRT), combined with small coincidence windows. To minimize the pile-up inside the detector elements, a one-to-one coupling between small size crystals and the photosensors must also be adopted. Compared with the approaches of light sharing and/or monolithic crystals, normally used in preclinical PET, the one-to-one coupling reduces the number of hits per channel (also allowing the use of existing readout ASICs at the mentioned high activities), but increases the number of readout channels.

A CRT of 300 ps FWHM is envisaged in SAFIR, with a corresponding coincidence window of the same size. A good spatial resolution of the order of 2.0 mm FWHM is also required. In terms of spatial constraints, the insert must have a maximum outer diameter of 20 cm and leave a free inner bore diameter of at least 12 cm, to house the animal in its bed structure and the RF coils. A high data rate, of the order of 10 kHz per  $\text{mm}^2$  of detector area is computed from solid angle considerations and probability of interaction (and also verified by simulations).

### 2.3. Detector design

SAFIR relies on a conventional cylindrical PET geometry, with radially oriented LSO-based scintillating crystals arranged in modules, and coupled one-to-one to arrays of SiPM sensors, readout by existing fast readout ASICs. Modules are arranged in rings, with minimal gaps. Several rings are axially stacked to provide the full field of view coverage.

In the so-called *reference design* (Fig. 1), a specific geometry has been fixed, driven by the availability on the market of the detector components (crystals and photosensors) with dimensions able to

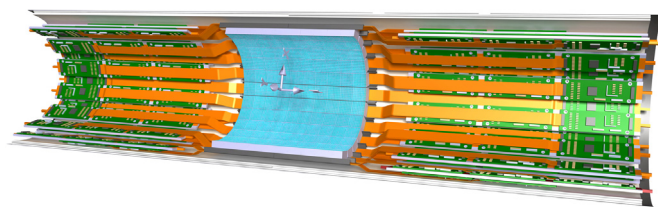


**Fig. 1.** Schematic view of one half of the SAFIR detector in the reference design. The central part hosts crystals and photo-sensors; the left and right compartments include readout and data acquisition electronics.

meet the detector requirements. In the reference design geometry, polished LYSO crystals of  $(2.1 \times 2.1 \times 12)\text{mm}^3$  are arranged in an  $8 \times 8$  geometry, with 3 M ESR foil separator among the channels. The crystals matrices are optically glued to arrays of  $8 \times 8$  SiPMs (of the type Hamamatsu S13361–2050AE-08). The detector features 10 rings, with 24 modules per ring, resulting in 182 mm axial coverage, 135 mm inner diameter, and 15,360 readout channels.

The reference design is the one currently adopted in the simulations, and represents one possible realistic detector layout for the future. It is also the geometry that will be likely adopted in the implementation of a first single ring PET. Further optimisations in the exact crystals dimensions, photosensors type and arrangement could still be envisaged for the final detector layout.

The insert is supported by a hollow fiberglass composite cylindrical structure (120 mm diameter) with an external coverage. The two concentric cylindrical shells and their end pieces will serve not only as mechanical structure but also as an RF screen.

## 3. Status of the experiment and first results

Both hardware and software activities are pursued, towards the finalisation of the SAFIR detector and the assessment of its performance. The project is staged: small scale prototypes will drive the decision on the detector components to be used; this will be followed by the construction of one single ring that could be already used for dynamic tomographic reconstruction (although at significantly reduced sensitivity); finally the entire insert will be constructed.

### 3.1. Simulations

The full SAFIR detector is simulated in the reference design geometry, using a custom developed simulation framework based on Geant4 [7]. A conservative Gaussian time smearing of  $\sigma \sim 150$  ps (corresponding to CRT  $\sim 500$  ps FWHM) is applied to the hits, as well as an energy blurring of  $\Delta E/E \sim 20\%$  FWHM (at 511 keV). NEMA standard [8] prescriptions are followed to define the performance of the detector and in particular its Noise Equivalent Count Rate (NECR), spatial resolution and sensitivity. The results of the simulations have been detailed in a dedicated publication [9]. In summary: the excellent coincidence timing resolution combined with an optimized short coincidence window (402 ps), and the high sensitivity (3.6% peak value, at photopeak energy window) allow us to suppress the contribution from the random events at activities as high as 500 MBq, while achieving a NECR significantly bigger than the one expected at the activities commonly employed in pre-clinical PET imaging ( $\sim 50$  MBq). Spatial resolutions of the order of 2 mm FWHM are obtained at the center of the scanner.

The quoted sensitivity refers to photoelectric absorption events only, not recovering any Inter-Crystal Scattering (ICS), which is however important, given the small crystal size. Preliminary

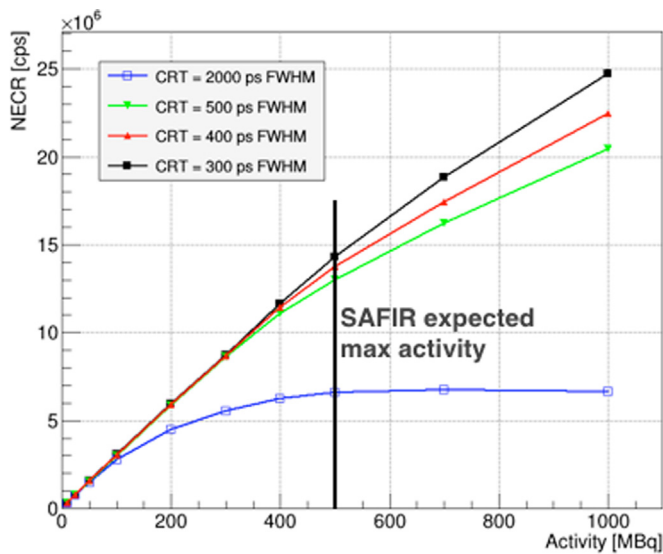


**Fig. 2.** Noise Equivalent Count Rate (NECR) curves for simulated data in the SAFIR reference design geometry, at different Coincidence Resolving Times (CRT) values. For simplicity, the adopted coincidence window in this study equals the CRT value.

studies indicate a sensitivity improvement by more than a factor 2 when ICS events in the same matrix are not discarded.

The crucial role of excellent CRT in the detector performance is highlighted by the results of Fig. 2, where NECR is computed for different coincidence timing resolutions. It is shown that the feasibility of SAFIR to handle high activities can be ensured only with CRT at the level of a few 100's ps.

### 3.2. Reconstruction

Tomographic image reconstruction is provided using the STIR [10] software framework. A custom multiple window coincidence sorter is applied on the simulated data and sinograms are produced from coincidence list-mode data, on which either analytical or iterative algorithms are applied.

Fig. 3 shows the example of the reconstructed image of a Derenzo phantom (with diameters of the spheres ranging from 4 to

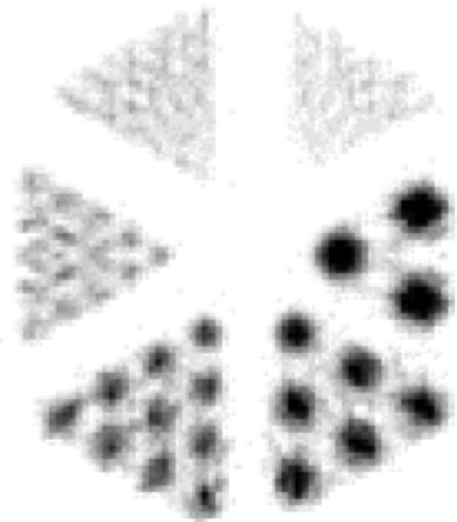


**Fig. 3.** Reconstructed image of a Derenzo phantom, for 1 s of simulated data, with 500 MBq total activity into the spheres structures (with diameters: 4 mm, 3.2 mm, 2.4 mm, 1.6 mm, 1.2 mm, 1.0 mm) and no background. Data are reconstructed using the Ordered Subset Maximum a posteriori one step late iterative reconstruction algorithm in STIR (OSMAPOS, 1 subset).

**Table 1**

List of available and tested samples of crystals (as individual ones and/or as matrices) for dedicated lab measurements.

Producer	Crystal type	1.5 mm side single crystal	3.1 mm side single crystal	4 × 4 matrices 3.1 mm side pitch 3.2 mm
AGILE	LYSO	X	X	X
SiPAT	LSO	X	–	X
SiPAT	LSO:Ca	X	–	–
Hamamatsu	LFS	X	X	X
Hilger	LYSO	X	X	X

1 mm), achieved in the best case scenario of 500 MBq activity entirely distributed into the spheres structures (i.e. with no background, which does not represent a realistic situation). As expected by the size of the crystals and by the demonstrated spatial resolution, spheres down to 2.4 mm are easily resolved, while it is challenging for the 1.6 mm ones or smaller.

### 3.3. Characterisation of the hardware components

Efforts towards the choice of the detector components focused so far on the following three major areas: (a) scintillator crystal properties; (b) SiPM type; (c) readout ASICs for the SiPMs readout.

Different L(Y)SO crystal samples from various producers (see Table 1) have been compared, both in terms of light yield and CRT performance. Individual crystals were procured, in two different sizes of  $(1.5 \times 1.5 \times 12) \text{ mm}^3$  and  $(3.1 \times 3.1 \times 12) \text{ mm}^3$ . Also matrices of  $4 \times 4$  assemblies of  $(3.1 \times 3.1 \times 12) \text{ mm}^3$  crystals with 100  $\mu\text{m}$  separation among the channels (65  $\mu\text{m}$  ESR foil, plus glue), from the same producers, were tested. As photosensors, different SiPM from Hamamatsu (MPPC), both as individual sensors and in a  $4 \times 4$  array arrangement, were used (see Table 2).

For a direct relative comparison, the measurements were performed in reproducible setups, however not optimised (e.g air coupling, instead of grease or glue; no cooling, but only a stabilised temperature around room conditions; no wrapping around the crystals, unless explicitly tested). Different acquisition modes were used, depending on the target measurement: a fully analogue readout chain, based on a charge integrating CAEN V792 QDC, for light yield comparison; a coincidence setup of two tiles of digital SiPM [11], for CTR comparison.

Different Hamamatsu MPPCs have been tested with respect to their saturation response. In particular the behaviour of the 50  $\mu\text{m}$  cells size samples is compared with the one of 25  $\mu\text{m}$  of larger linearity but smaller PDE (photon detection efficiency), for the same class of sensors (S12572). Standard Hamamatsu SiPM developments (S12572) are also compared with the newest available samples (S13082) featuring a much lower cross talk. Measurements have been made using crystals of small cross sectional size  $(1.5 \times 1.5) \text{ mm}^2$ , fully contained in the  $(3 \times 3) \text{ mm}^2$  sensor area (Fig. 4). The usage of small size crystals reduces any misalignment effect, but obviously entails a different saturation response with respect to the one expected in the SAFIR reference geometry,

**Table 2**

List of SiPM sensors used for dedicated lab measurements.

SiPM type	Sensor size ( $\text{mm}^2$ )	Cell size ( $\mu\text{m}$ )	nr cells/ sensor	Single/array
S12572–050C	$(3 \times 3)$	50	3600	single
S12572–025C	$(3 \times 3)$	25	14,400	single
S13082–050CS	$(3 \times 3)$	50	3600	single
S12642–0404PB–50 (X)	$(3 \times 3)$	50	3600	array, $4 \times 4$

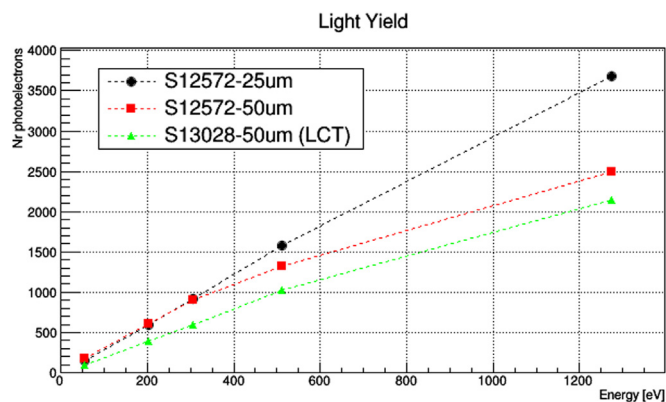


**Fig. 4.** Light yield (in terms of detected number of photoelectrons) as a function of the  $\gamma$  energy deposited in one sample of scintillator crystal (type LSO by SIPAT,  $(1.5 \times 1.5 \times 12)$  mm<sup>3</sup>, wrapped in ESR) coupled to different types of SiPM (50 vs. 25  $\mu$ m cell size; standard vs. low cross talk devices).

because of the lower number of cells covered by the crystal area. For this same reason, the typical light yields shown in Fig. 4, corresponding to about 1000–1500 pe at 511 keV, must be considered only as an indication of the expected light yield in SAFIR.

Additional results on the tests performed on SiPMs and crystals can be summarized as follows: (a) effect of calcium codoping on scintillators performance: A 25% improvement in CRT is registered for the SIPAT LSO:Ca (featuring a 0.4% Ca-codoping with respect to the standard LSO crystal of the same producer). This is due to a reduced decay time of the scintillator (34 ns vs. 42 ns of standard LSO), at the expense of a 10–15% reduction in the measured light yield. (b) Impact of wrapping and optical coupling: single crystals are tested unwrapped and without optical coupling with the photosensors – for simplicity and reproducibility reasons. Wrapping the crystal into a 65  $\mu$ m ESR foil and using an optical grease (Bicron BC-630) in the crystal/SiPM interface, increases by 30% the overall light yield. (c) Different crystal producers: a clear ranking among the producers could be established in terms of the registered light yields, with AGILE being the one that provides higher output crystals. This is confirmed both on the individual samples and with the matrices measurements. An improved light yield in the scintillators – with the same decay time i.e. except for Ca codoping crystals – directly translate into better CRT.

In the reference design, LYSO crystal matrices from AGILE will be employed. Crystals will be wrapped, also for optical separation among channels, and glued to the SiPMs. Photodetector arrays of the type Hamamatsu S13361–2050AE-08 will be used. They represent the analogous of the tested low cross talk samples, in form factor of arrays.

For what concerns the SiPMs readout chip, the STiC [12] and the TOPPET [13] 64-channel readout ASICs have been extensively tested, both with low activity <sup>22</sup>Na sources, and in a high rate test setup, where two matrices (crystals and SiPM) were exposed – in coincidence – to a high activity phantom (FDG filled, at Zürich University Hospital). Both chips have demonstrated rate

capabilities that exceed the needs ( $>40$  kHz/channel for  $(2 \times 2)$  mm<sup>2</sup> detector size) and STiC meets the 300 ps requirement in the CRT (FWHM). Details and results from the high rate test will be the subject of a forthcoming publication and will not be reported here.

Preliminary high rate tests on a compact  $\gamma$  detection module, with LYSO crystals and FBK SiPM sensors readout via the PETA5 ASIC [14] in a hybrid flip-chip mounted assembling [15] also show promising performance for the SAFIR readout.

#### 4. Conclusions and outlook

In the rapidly evolving scenario of hybrid PET/MRI instrumentation, SAFIR represents a novelty, in which extremely short time granularities ( $\sim$ few seconds) must be achieved with extremely high injected activities ( $\sim$  500 MBq). Without being a Time-Of-Flight (TOF) PET development, excellent time resolutions ( $\sim$  300 ps) must be ensured. High rate capability per channel ( $\sim$  10 kHz/mm<sup>2</sup>), high number of readout channels, and consequent huge data throughput and fast DAQ are additional challenges to be faced.

The feasibility of the SAFIR concept has been demonstrated by simulations, and also by initial measurements on possible detector components, which have also already driven some of the decisions in terms of detector implementation.

STiC and PETA ASICs are considered valid options for the SAFIR readout, meeting the requirements. Two prototypes will be built, each consisting of two modules in coincidence; one will use two modules in the reference design geometry, readout by two STiC chips, the other will feature two PETA modules (detectors and readout). The prototypes will be tested at high rate and inside the bore of the MR scanner by end 2016.

#### References

- [1] B.J. Pichler, et al., *J. Nucl. Med.* 51 (3) (2010) 333–336; T. Beyer, et al., *Insight Imaging* 2 (2011) 235–246; H. Zaidi, A. Del Guerra, *Med. Phys.* 38 (10) (2011); H. Zaidi, et al., *Med. Phys.* 34 (5) (2007).
- [2] D.W. Townsend, *J. Nucl. Med.* 42 (2001) 533; P.E. Kinahan, *Med. Phys.* 25 (October (10)) (1998) 2046–2053.
- [3] G. Wagenknecht, et al., *Magn. Reson. Mater. Phys.* 26 (2013) 99–113.
- [4] S. Vandenberghe, P.K. Marsden, *Phys. Med. Biol.* 60 (2015) R115–154.
- [5] E. Roncali, S. Cherry, *Annals of Biomedical Engineering*, vol. 39, no. 4, 2011; V. Spanoudaki et al., *J. Instrum.* 2 (2007) P12002.
- [6] M. Judenhofer, S. Cherry, *Semin. Nucl. Med.* 43 (1) (2013) 19–29.
- [7] S. Agostinelli, et al., *Nucl. Instrum. Methods A* (2003) 506; J. Allison, et al., *IEEE Trans. Nucl. Sci.* 53 (1) (2006) 270.
- [8] NEMA Standard Publication NU 4-2008.
- [9] R. Becker et al. *IEEE NSS-MIC 2015 Conference Record M4CP-362*.
- [10] K. Thielemans, et al., *Phys. Med. Biol.* 57 (4) (2012) 867.
- [11] T. Frach et al., 2009 IEEE NSS MIC Conference Record N28-005.
- [12] T. Harion et al., *J. Instrum.* 9 C02003 (2014).
- [13] M. Rolo et al., *J. Instrum.* 8 C02050 (2013).
- [14] P. Fischer, et al., *IEEE Trans. Nucl. Sci.* 56 (3) (2009) 1153.
- [15] I. Sacco et al. *Nucl. Instrum. Methods A* (2016) 824.